Published in final edited form as:

J Am Chem Soc. 2015 November 11; 137(44): 14173–14179. doi:10.1021/jacs.5b09158.

Amplifying the Sensitivity of Zinc(II) Responsive MRI Contrast Agents by Altering Water Exchange Rates

Jing Yu[†], **André F. Martins**[†], **Christian Preihs**[‡], **Veronica Clavijo Jordan**[‡], **Sara Chirayil**[‡], **Piyu Zhao**[†], **Yunkou Wu**[‡], **Khaled Nasr**[‡], **Garry E. Kiefer**[†,§], and **A. Dean Sherry**[*,†,‡]

[†]Department of Chemistry, University of Texas at Dallas, P.O. Box 830668, Richardson, Texas 75083, United States

[‡]Advanced Imaging Research Center, The University of Texas, Southwestern Medical Center, 5323 Harry Hines Boulevard, Dallas, Texas 75390, United States

[§]Macrocyclics, Inc., 1309 Record Crossing, Dallas, Texas 75235, United States

Abstract

Given the known water exchange rate limitations of a previously reported Zn(II)-sensitive MRI contrast agent, GdDOTA-diBPEN, new structural targets were rationally designed to increase the rate of water exchange to improve MRI detection sensitivity. These new sensors exhibit fine-tuned water exchange properties and, depending on the individual structure, demonstrate significantly improved longitudinal relaxivities (r_1). Two sensors in particular demonstrate optimized parameters and, therefore, show exceptionally high longitudinal relaxivities of about 50 mM^{-1} s^{-1} upon binding to Zn(II) and human serum albumin (HSA). This value demonstrates a 3-fold increase in r_1 compared to that displayed by the original sensor, GdDOTA-diBPEN. In addition, this study provides important insights into the interplay between structural modifications, water exchange rate, and kinetic stability properties of the sensors. The new high relaxivity agents were used to successfully image Zn(II) release from the mouse pancreas *in vivo* during glucose stimulated insulin secretion.

Graphical abstract

[*]**Corresponding Author:** dean.sherry@utsouthwestern.edu; sherry@utdallas.edu.

Supporting Information

The Supporting Information is available free of charge on the ACS Publications website at DOI: 10.1021/jacs.5b09158. General methods, supplementary schemes, synthetic protocols, and analytical data for the new compounds. (PDF)

Notes

The authors declare no competing financial interest.

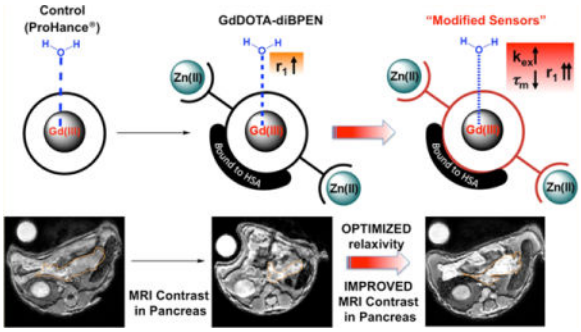

1. INTRODUCTION

As the second most abundant transition metal in mammalian tissue, divalent zinc (Zn(II)) plays a critical role in many cellular processes including structural, catalytic, and signal transduction processes.[1] The total concentration of Zn(II) in blood is 12–16 μM, mostly in chelated, protein-bound forms.[2] Zn(II) concentrations are particularly high in the pancreas,[3] prostate,[4] and brain,[5] all tissues that require Zn(II) for signal transduction. Pancreatic beta cells store insulin with two equivalents of Zn(II) in granules and release Zn(II) with insulin in response to an increase in plasma glucose. Upon release of insulin, the local concentration of Zn(II) in the vicinity of the beta cells rises transiently to ~450 μM[6] and may signal other cells in the same islet.[7] Zn(II) is tightly regulated by multiple different transporters and imbalances in Zn(II) content in these various tissues is associated with diabetes, Alzheimer's disease, and prostate cancer.[8] For more than two decades, extensive efforts have been devoted to the development of optical sensors for detection of free Zn(II) ions.[9,10] Optical Zn(II) sensors offer an appropriate detection sensitivity but show limited applicability for monitoring Zn(II) levels *in vivo*.[11] Thus, optical-based Zn(II) sensors have been largely restricted to cell-based imaging. Magnetic resonance imaging (MRI) is an attractive modality for imaging physiology *in vivo* because tissue penetration is not a limiting factor. Unfortunately, MRI is inherently much less sensitive than optical imaging, which is why MR reporter molecules cannot be detected directly but rather must be detected indirectly through the abundant water protons. The first Zn(II) responsive MRI contrast agent reported in 2001[12] was designed to detect a change in water access to the inner-sphere of a Gd(III) ion upon Zn(II) binding. Since then, several other designs based on changes in q in response to Zn(II) have been reported,[13–16] but none show particularly large changes in r_1 relaxivity in response to Zn(II). Even so, a Mn(II) porphyrin derivative did show signal enhancement in brain regions known to contain the highest Zn(II) levels, but this required direct injection of the agent.[14] This observation demonstrated the feasibility of detecting Zn(II) in tissues by T_1-weighted imaging. In 2009, a new type of Zn(II) sensor design based on a change in molecular rotation, τ_R, was reported.[17] Upon binding of two Zn(II) ions to the high affinity *N,N*-bis(2-pyridyl-methyl)ethylenediamine (BPEN) sites on GdDOTA-diBPEN **1** (cf. Figure 1), the resulting ternary GdL-$(Zn)_2$ complex binds to site 2 of subdomain IIIa in human serum albumin (HSA). This results in slowing of molecular rotation and a change in r_1 from 5.0 mM^{-1} s^{-1} to 17.5 mM^{-1} s^{-1} at 0.47 *T*. Although the increase in r_1 is not nearly this large at 9.4 *T*, where subsequent mouse imaging experiments were performed, even a 2-fold change in r_1 was sufficient to detect Zn(II) ions coreleased with insulin from pancreatic β-

cells.[18] The approach taken in that imaging study was to administer a dose of GdDOTA-diBPEN **1** such that its extracellular concentration is near the detection limit of MRI (i.e., 0.025 mmol/kg) and then assign any increase in image intensity in the pancreas after a bolus of glucose, to an increase in local Zn(II) released from β-cells. Although the method proved useful for detecting the expansion of pancreatic tissue in mice fed a high fat diet over 12 weeks, it would be highly desirable to modify the structure of GdDOTA-diBPEN **1** to amplify the sensitivity of the agent for detecting Zn(II) release from secretory tissues.

It is well known that the water exchange rate (k_{ex}) in bis-amide derivatives like GdDOTA-diBPEN **1** (cf. Figure 1) is typically 20–50 fold slower than that considered optimal for achieving a maximal increase in r_1 when the agent binds to a macromolecule.[19] This suggested to us that the r_1 relaxivity of GdDOTA-diBPEN **1**-$(Zn(II))_2$ when bound to albumin is likely limited by slow k_{ex}. Based on other known τ_M ($\tau_M = k_{ex}^{-1}$) values of modified derivatives of GdDOTA, a series of new complexes were designed with a goal of increasing the rate of water exchange from the inner coordination sphere of the Gd(III) ion while preserving the Zn(II) binding sites and, hopefully, albumin-binding characteristics of GdDOTA-diBPEN **1**. In compound Gd-**2**, two phosphinate groups were introduced as oxygen donors to introduce greater steric hindrance around the Gd(III)-water binding site.[20] This should in principle increase the rate of water exchange. The two piperazine units in compound Gd-**3** were introduced to increase the population of the twisted square antiprism (TSAP) isomer, a coordination isomer known to display much faster water exchange.[21,22] In compounds Gd-**4**, Gd-**5**, and Gd-**6**, an extra methylene carbon was included in either an acetate (Gd-**4**) or acetamide (Gd-**5** and Gd-**6**) side-chain, a modification also known to increase steric hindrance around the Gd(III)-water coordination site.[23] The impact of expanding the chelate ring size on τ_M can be rather dramatic. For example, a structural analogue of GdDOTA bearing an extra methylene carbon on one acetate arm exhibits a 15-fold faster water exchange rate compared to GdDOTA.[23,24] Given this prior information, compounds Gd-**4**, Gd-**5**, and Gd-**6** were predicted to display considerably faster water exchange rates.

2. RESULTS AND DISCUSSION

2.1. Synthesis of Sensors

GdDOTA-diBPEN **1** was prepared as reported previously.[17] The macrocyclic Gd complexes, Gd-**2** to Gd-**6**, in Figure 1 were prepared using synthetic procedures fully described in Supporting Information. Each Gd(III) complex was purified and characterized using standard methods (preparative HPLC, ^{1}H NMR, ^{13}C NMR, and LC-MS). Those details can also be found in the Supporting Information (SI) section.

2.2. ^{17}O NMR Measurements

To evaluate the principal physical parameters that govern r_1 relaxivity, 25 mM samples of each Gd(III) complex were prepared in 5%-enriched ^{17}O water for ^{17}O T_1 and T_2 measurements over the temperature range 277–333 K. Figure S2 in SI summarizes the temperature dependence of the reduced ^{17}O chemical shifts ($\Delta\omega_r$), transverse ($1/T_{2r}$) and longitudinal ($1/T_{1r}$) relaxation rates for all six complexes. τ_R and k_{ex} were determined by

fitting the longitudinal (T_{1r}) and transverse (T_{2r}) data simultaneously to paramagnetic relaxation theory.[25,26] The ^{17}O transverse relaxation rates for GdDOTA-diBPEN **1** increase with temperature above 333 K, indicating that water exchange lies in the slow-to-intermediate exchange regime where $1/T_{2r}$ provides a direct measure of k_{ex}. The $\tau_M = 1/k_{ex}$ value obtained for GdDOTA-diBPEN **1** at 298 K (1362 ns) is consistent with previous observations that replacement of carboxylate by an amide typically decreases the rate of water exchange by 3–4 fold. The τ_M values found for Gd-**4** and Gd-**5** (190 ± 7 and 130 ± 2 ns, respectively) were ~7-fold and ~11-fold shorter than the τ_M found for GdDOTA-diBPEN **1**, and even modestly shorter than the τ_M of GdDOTA (243 ns).[26] This nicely demonstrates that introducing one extra carbon spacer into either the acetate or amide coordinating side-chain had the anticipated impact of increasing the rate of water exchange. Clearly, introducing an extra methylene carbon in the acetamide side-chain had a larger impact on water exchange than expansion of the acetate side-chain. This effect was further amplified in Gd-**6**, where extending both amide side-chains by one carbon decreased τ_M by another ~35-fold to 3.7 ± 0.1 ns.

The τ_M values summarized in Table 1 show that all of the new Zn(II) sensors display faster water exchange than GdDOTA-diBPEN **1**. The largest change was observed for the phosphinate derivative (Gd-**2**) and the bis-amide complex with extra methylene carbons on both appended amide side-chain ligating groups (Gd-**6**). According to paramagnetic relaxation theory, complexes with τ_M values in this range (<5 ns) are too short to achieve an optimal r_1 when bound to a protein. The τ_M value measured for Gd-**3** (8.7 ± 0.1 ns) was closest to the value considered optimal for achieving maximal r_1 relaxivity.[19] This finding suggests that insertion of the bulky cyclohexane groups likely increased the population of TSAP isomer. To verify that this is indeed the origin of this increase in τ_M, a sample of Eu-**3** was prepared for high resolution ^1H NMR. The spectrum (cf. Figure S4.1 in SI) verified that the fraction of TSAP isomer in this complex was ~80%, much larger than the TSAP fractions in Eu-2 (~66%), Eu-4 (~5%), or Eu-5 (<5%), or EuDOTA-diBPEN **1** (~40%) (cf. Figures S4.2–S4.4 in SI).[17] Finally, sensors Gd-**4** and Gd-**5** with one extra methylene carbon inserted into one ligating side-chain displayed water exchange rates about 10-fold faster than GdDOTA-diBPEN **1**. This series illustrates that one can use a variety of different coordination chemistry principles to modify water exchange rates in Gd(III) complexes. The τ_{RO}^{298} values for these complexes calculated from the ^{17}O T_1 data were all in the range 0.3–0.4 ns, indicating that these complexes rotate more slowly than GdDOTA, as one would expect on the basis of molecular weight.[27,28] The inner-sphere q value of each complex was estimated from the ^{17}O chemical shift of the fully bound water molecule (δ_μ).[29] All q values obtained were close to 1, except for sensor Gd-**2**, where q was found to be equal to 0.4 (Table 1). This likely reflects the presence of multiple coordination isomers in solution, perhaps one with $q = 0$ (60%) and one with $q = 1$ (40%). Complexes with $q = 0$ have been observed previously in a variety of phosphonate and phosphinate complexes.[30] To confirm the q values measured from ^{17}O NMR, q was also evaluated by luminescence lifetime measurements on the corresponding Eu(III) complexes. Those measurements gave values of 0.4 and 0.9 ± 0.2 for Eu-**2** and Eu-**6**, respectively, indicating the q values obtained by ^{17}O NMR on the Gd complexes are in good agreement with those measured by luminescence lifetime methods.

2.3. Relaxivity Measurements

The r_1 relaxivity of each new sensor in the absence and presence of Zn(II) and HSA were compared with the corresponding values for GdDOTA-diBPEN **1** in Table 1. In the absence of Zn(II) and HSA, the r_1 values of complexes roughly parallel the molecular weights of the complexes in solution, with the possible exception of Gd-**6**. Given the fact that q for Gd-**6**, as measured by two different methods, seems to be near 1 and the complex was pure by all analytical measurements, the origin of the unusually low r_1 relaxivity of this complex remains unknown. Like GdDOTA-diBPEN **1**, the r_1 relaxivities of the new sensors did not change significantly upon addition of two equivalents of Zn(II) (as $ZnCl_2$) but did increase dramatically upon addition of both Zn(II) and a physiological amount of HSA (600 μM). This indicates that the five new Zn(II) sensors reported here retain their ability to bind to HSA in the presence of Zn(II) ions and binding significantly slows molecular rotation and increases r_1. Relaxivity theory predicts that the r_1 of each Gd(III) sensor-Zn(II)-HSA adduct will depend upon the water exchange rates with the complexes bound to HSA.[19] Unfortunately, we were unable to use ^{17}O NMR techniques to measure τ_M for the HSA-bound sensors because of limitations in concentration imposed by the protein. Despite this limitation, it is useful to compare the experimental r_1 values measured in the presence of HSA with the τ_M values measured in the absence of Zn(II) and protein (Figure 2). If the rate of water exchange is unaltered upon binding of these agents to HSA, then the r_1 values measured in aqueous solution in the absence of HSA should reasonably fit the theoretical plots shown in Figure 2. Three of the six complexes (GdDOTA-diBPEN **1**, Gd-**4**, and Gd-**5**) agree reasonably well with theory, whereas three other complexes (Gd-**2**, Gd-**3**, and Gd-**6**) do not. To validate the positioning of the data point for each complex on this curve, additional r_1 measurements were performed in the presence of Zn(II) and HSA at 323 K (Table S2 in SI). As expected, the r_1 relaxivities of GdDOTA-diBPEN **1**, Gd-**4** and Gd-**5** were higher at 323 K, whereas the r_1 relaxivities of Gd-**2**, Gd-**3**, and Gd-**6** were lower. Given the fact that the rate of water exchange should increase with temperature, this validates the positioning of the GdDOTA-diBPEN **1**, Gd-**4**, and Gd-**5** data on the “slow side” of the peak maximum of Figure 2 and Gd-**2**, Gd-**3**, and Gd-**6** on the “fast side” of this peak maximum. The observation that the data for GdDOTA-diBPEN **1**, Gd-**4**, and Gd-**5** fall at least near this theoretical curve suggests but does not prove that k_{ex} in these three complexes is not altered upon binding to HSA, whereas k_{ex} may differ when Gd-**2**, Gd-**3**, or Gd-**6** bind to the protein. It is also known that the r_1 relaxivity of Gd(III) complexes such as these are magnetic field dependent and the data in Table S3 in SI show that the r_1 relaxivities of GdDOTA-diBPEN, Gd-**4**, and Gd-**5** all decrease significantly between 0.5 and 9.4 T. The change in r_1 relaxivity is not large for the complexes in aqueous solution but is quite dramatic for the Gd-**4** and Gd-**5** when bound to HSA. These data suggest that there should be a sensitivity advantage in detecting Zn(II) release from the pancreas at lower magnetic fields (1.5 T or lower), but this advantage could be partially offset by the inherent lower ^1H sensitivity at the lower magnetic field.

2.4. Albumin-Binding Measurements

It is well known that HSA can bind many different types of substrates via site 1 or 2 of subdomain IIA or IIIA. Both are characterized by hydrophobic pockets, surrounded by a

positively charged external surface.[26] Studies indicate that, in the case of amphiphilic molecules, like MS-325 and MP-2269, the hydrophobic side-chains in these molecules bind in these hydrophobic pockets on the protein, whereas the Gd(III) chelate has minimal interactions with the protein surface.[31–34] Nevertheless, it has been found that the rate of water exchange between a Gd(III) complex can be reduced quite substantially upon binding of the agent to HSA.[31] Interestingly, it has also been shown that the rate of water exchange in various Ln(III) derivatives of MS-325 is quite sensitive to relatively minor structural differences between albumin from different mammalian sources[35] and when various Mn(II) complexes bind to albumin.[36]

$$R_1^{\mathrm{pobs}} = 10^3 \times \left\{ (r_1^f \cdot c_1) + \frac{1}{2}(r_1^c - r_1^f) \times (n \cdot c_{\mathrm{HSA}} + c_1 + K_A^{-1}) - \sqrt{(n.\, c_{\mathrm{HSA}} + c_1 + K_A^{-1})^2 - 4 \cdot n \cdot c_{\mathrm{HSA}} \cdot C_1)} \right\}$$

(1)

For the Zn(II) sensors presented here, HSA binding takes place mostly by the electrostatic interaction between the Zn(II)-DPA subunits and the tyrosine residue Y411 in the pocket site 2.[37] The binding affinity of each Zn(II) sensor to HSA was estimated by proton relaxation enhancement (PRE) titrations, a relaxometric technique commonly used to determine the dissociation constants ($K_D = 1/K_A$) for binding of Gd(III) complexes to HSA.[17] This experiment consists of measuring the proton relaxation rates R_{1obs} at increasing concentrations of the protein at a fixed concentration of complex (Figure 3). Data such as these were fitted to eq 1, where r_1^f and r_1^c are the proton relaxivities of the free and the bound state, c_{HSA} and c_1 are the concentrations of HSA and complex, respectively, and n is the number of binding sites on the protein. Assuming that the complexes only bind to HSA-binding site 2 of subdomain IIIA ($n = 1$), a fit of the data to eq 1 revealed relatively strong binding for **1**, Gd-**4**, and Gd-**5** with HSA (K_D ~ 42–48 μM), in good agreement with literature values,[17] whereas Gd-**2**, Gd-**3**, and Gd-**6** exhibit lower affinities with HSA (383 ± 60 μM, 227 ± 52 μM, 130 ± 25 μM, respectively). This suggests that the length and flexibility of the side-chains between the Gd(III) and the Zn(II)-DPA units have a substantial influence on the binding interactions on HSA. Interestingly, **1**, Gd-**4**, and Gd-**5**, the three complexes with the highest affinity for HSA, fall onto the theoretical r_1 curve of Figure 2, whereas Gd-**2**, Gd-**3**, and Gd-**6**, those with the lowest affinity for HSA, do not. The abnormally low r_1 of Gd-**2** can be partly explained by this complex having a q value less than 1 (Table 1 and Figure 2, mark Gd-**2′**), whereas Gd-**3** and Gd-**6** must fall off this relationship for other reasons. It is also interesting to observe that these same three complexes have a weaker binding affinity for HSA. Given the fact that Gd-**3** favors the TSAP form in solution, it is reasonable to assume that this complex may favor a different coordination isomer when bound to the protein and thereby may have quite a different water exchange rate. Similarly, the side-chain groups on Gd-**6** are highly flexible, so this complex may also adopt a different structure when bound to HSA. An alternative explanation is that protein donor atoms displace the inner-sphere water molecule in Gd-**6** to give a $q = 0$

complex when bound to HSA. This mechanism was suggested for some other GdDO2A derivatives when bound to HSA to explain their unexpectedly low bound r_1 values.[38]

With the exception of Gd-**6**, the other four new complexes displayed higher r_1 values when bound to HSA than GdDOTA-diBPEN **1**, consistent with faster water exchange. Gd-**4** and Gd-**5** in particular exhibit remarkably high relaxivities of 47.6 ± 1.2 and 50.1 ± 1.2 mM^{-1} s^{-1}, respectively, when bound to Zn(II) and HSA (Table 1). These values, about 3-fold higher than the corresponding r_1 value of GdDOTA-diBPEN **1**-Zn(II)-HSA, suggest that detection of Zn(II) released from the pancreas in response to glucose stimulation should be about 3-fold more sensitive when using these newer agents at 0.47 *T*. This difference, however, would not be nearly as large at 9.4 *T*.

2.5. In Vivo Imaging of Glucose-Stimulated Insulin and Zn(II) Release from the Mouse Pancreas

We previously reported that GdDOTA-diBPEN 1 detects release of Zn(II) ions from pancreatic β-cells in response to an increase in blood glucose by MRI.[18] Given the fact that two of the new Zn(II) sensors, Gd-**4** and Gd-**5**, display about a 3-fold improvement in r_1 relaxivity upon binding to Zn(II) and HSA *in vitro* in comparison to GdDOTA-diBPEN **1**, additional *in vivo* imaging experiments were performed in mice to evaluate whether this enhanced *in vitro* relaxivity translates to improved signal enhancement of the pancreas *in vivo*. In separate experiments, three different agents were infused into C57Bl/6 mice using an identical infusion protocol to compare their effectiveness. Figure 4 summarizes the imaging protocol (top panel) and shows typical T_1-weighted MR images of mice in axial view at 10–15 min after stimulation of Zn(II) release by glucose. Initially, each agent was infused at 5 μL/min for ~30 min while continuously monitoring the image intensity of the kidneys. Once constant enhancement of the kidneys was observed, 50 μL of 20% w/v D-glucose was injected into the intraperitoneal (IP) space while continuously monitoring the pancreas by sequential T_1-weighted MRI. Maximal enhancement was observed at 10–15 min after glucose injection correlating with our previous reports of zinc/insulin corelease after stimulation.[18] Figure 4 summarizes the percent signal enhancement of selected ROIs of the pancreas 11 min after glucose stimulation. Although significantly higher signal enhancement of the pancreas was detected during infusion of GdDOTA-diBPEN **1** (as reported previously) and Gd-**5** when compared to Gd-HPDO3A, the percent signal enhancement differences between GdDOTA-diBPEN and Gd-**5** did not reach statistical significance ($p < 0.125$). There may be several reasons why the higher *in vitro* r_1 of Gd-**5** did not translate to greater tissue enhancement in vivo including: (1) given the fact that the pancreas is not a solid organ but rather a thin tissue, there are likely significant variations in selection of identical ROI's in every mouse and (2) the r_1 difference between GdDOTA-diBPEN **1** versus Gd-**5** when bound to Zn(II) and HSA is only 1.3-fold greater at 9.4 *T* compared the much larger difference observed at 0.47 *T*. The fact that we do detect a trend toward higher signal enhancement using Gd-**5** compared to GdDOTA-diBPEN **1** (Figure 4) is encouraging because it suggests that the new higher relaxivity agents, Gd-**4** and Gd-**5**, will show significantly improved signal enhancement upon Zn(II) release from the pancreas at clinical imaging fields.

2.6. Kinetic Inertness

Thermodynamic stability and kinetic inertness are two critical parameters for the successful translation of new agents into clinical medicine. The new agents presented here based on the DO2A scaffold typically exhibit stability constants in the range of log K_{ML} = 20 or higher.[39] Therefore, thermodynamic stability should not be a limiting factor. Kinetic inertness, arguably the more important factor in determining the viability of these complexes for clinical translation, was assessed by use of a published transmetalation method.[40] Here, the Gd(III) complexes were incubated with four equivalents of Zn(II) in phosphate buffer (pH = 7), two equivalents of Zn(II) are expected to coordinate with the DPA subunits present in each sensor and the remaining two equivalents of Zn(II) are intended to gradually replace the Gd(III) from its macrocyclic binding site if the complex is kinetically labile on the time-scale of a few days. Any Gd(III) released by the macrocyclic ligands will in turn precipitate from solution as insoluble gadolinium phosphate, and as a consequence, the T_1 of the water protons will increase. The kinetic inertness of each new compound was compared with that of the FDA-approved contrast agent Magnevist (GdDTPA, cf. Figure 5). As anticipated, all six of the macrocyclic complexes were kinetically more inert than the noncyclic Gd(III) chelate Magnevist. In particular, Gd-**2** was the most inert complex in this series, with essentially no transmetalation occurring over 7 days. Gd-**3** and GdDOTA-diBPEN **1** exhibited similar kinetic inertness with their relaxation rates dropping only slightly in the beginning of the experiment. Gd-**4** and Gd-**5** were somewhat more labile but were still noticeably more inert than Magnevist. Gd-**6** was the most labile complex among this series. The combined data show that the coordinating phosphinate groups in Gd-**2** can dramatically stabilize the complex, whereas an extra methylene spacer in the carboxylate ligand results in reduced kinetic stability.

3. CONCLUSIONS

A series of Zn(II)-sensitive MRI sensors was designed to fine-tune the rate of water exchange from the inner-sphere of Gd(III) in order to maximize the r_1 of the complexes bound to Zn(II) and HSA. Two complexes in particular, Gd-**4** and Gd-**5**, displayed r_1 relaxivity values close to 50 $mM^{-1}s^{-1}$ at 0.47 T. This illustrates that optimizing the water exchange rates can be a successful molecular design strategy to construct more sensitive MRI contrast agents for Zn(II) detection. The 3-fold increase in r_1 measured for two of the new agents *in vitro* at 0.47 *T* did not result in significantly improved signal enhancement of the mouse pancreas *in vivo* at 9.4 T. Nevertheless, we anticipate that the higher r_1 relaxivity of these new agents will be much more evident when imaging larger animals at clinical imaging fields.

It should be noted that MR-responsive agents such as those described herein offer the possibility of detecting only qualitative changes in the amount of Zn(II) released from secretory tissues, not quantitative total Zn(II) concentrations in tissue. Nonetheless, MRI-based Zn(II) sensors such as these can provide added insights into physiological events occurring *in vivo* that are simply not available with other molecular imaging modalities. Given the fact that binding affinity of HSA for Zn(II) is ~30 nM[41] and the affinity of these BPEN-based Gd(III) complexes for Zn(II) is also around 33 nM,[2] one should consider the

relative concentrations of the agent (~50 μM) and HSA (~0.6 mM) in the extracellular space around β-cells to gain some insight into the various Zn(II) species that can potentially be formed upon release of Zn(II) ions from β-cells. The concentration differences between the Gd(III) sensor and HSA suggests that most of the Zn(II) released from β-cells should bind directly with HSA and not the Gd(III) sensor, assuming of course that the Zn(II) binding sites on HSA are not already occupied. The fact that HSA is considered to be a Zn(II) buffer and involved in delivery of Zn(II) to cells[42] and the fact that we observe image enhancement of the pancreas in response to glucose indicates that the Zn(II) binding sites on HSA must be largely occupied with Zn(II) before more ions are released from β-cells. This then allows the excess Zn(II) ions released from cells to bind to the Gd(III) sensor and subsequently enhance the MRI signal.

It is also important to point out that 4 of 5 of the new Gd(III) complexes reported here, like GdDOTA-diBPEN **1**, have an overall net charge of 1+ in the absence of Zn(II), yet seem to be well tolerated when infused into mice at the concentrations used here. Given the fact that positively charged Gd(III) complexes are generally considered toxic, our observations suggest that either the charge on these complexes is masked by associated counteranions *in vivo* or perhaps chemical toxicity will be revealed when these agents are infused at concentrations higher than those used here.

Supplementary Material

Refer to Web version on PubMed Central for supplementary material.

Acknowledgments

Financial support from the National Institutes of Health (P41-EB015908, R01-DK095416, and in part by the Harold C. Simmons Cancer Center through an NCI Cancer Center Support Grant, 1P30-CA142543), the American Diabetes Association (7-12-MN-76 and 7-12-IN-42), and the Robert A. Welch Foundation (AT-584) is gratefully acknowledged.

ABBREVIATIONS

q	hydration number
τ_R	rotational correlation time
τ_M	water residence lifetime
k_{ex}	water exchange rate
r_1	T1 relaxivity
r_{Gd-O}	gadolinium−water distance
T_{1e}	electronic relaxation time
TSAP	twisted square antiprism
DPA	di(2-picolyl)-amine

HSA	human serum albumin
K_D	dissociation constant
K_A	association constant
BPEN	*N,N*-bis(2-pyridyl-methyl)-ethylenediamine
DTPA	2-[bis[2-[bis(carboxymethyl)amino]-ethyl]amino]acetic acid

References

1. Maret W. Adv Nutr. 2013; 4:82–91. [PubMed: 23319127]
2. De Leon-Rodriguez L, Lubag AJM Jr, Sherry AD. Inorg Chim Acta. 2012; 393:12–23.
3. Chimienti F. Nutr Res Rev. 2013; 26:1–11. [PubMed: 23286442]
4. Kolenko V, Teper E, Kutikov A, Uzzo R. Nat Rev Urol. 2013; 10:219–226. [PubMed: 23478540]
5. Bush AI. Trends Neurosci. 2003; 26:207–214. [PubMed: 12689772]
6. Kim BJ, Kim YH, Kim S, Kim JW, Koh JY, Oh SH, Lee MK, Kim KW, Lee MS. Diabetes. 2000; 49:367–372. [PubMed: 10868957]
7. Li D, Chen S, Bellomo EA, Tarasov AI, Kaut C, Rutter GA, Li W. Proc Natl Acad Sci USA. 2011; 108:21063–21068. [PubMed: 22160693]
8. Myers SA, Nield A, Myers M. J Nutr Metab. 2012; 2012:173712–173725. [PubMed: 23304467]
9. Frederickson CJ, Kasarskis EJ, Ringo D, Frederickson RE. J Neurosci Methods. 1987; 20:91–103. [PubMed: 3600033]
10. Xu Z, Yoon J, Spring DR. Chem Soc Rev. 2010; 39:1996–2006. [PubMed: 20428518]
11. Weissleder R, Pittet MJ. Nature. 2008; 452:580–589. [PubMed: 18385732]
12. Hanaoka K, Kikuchi K, Urano Y, Nagano T. J Chem Soc Perkin Trans. 2001; 2:1840–1843.
13. Hanaoka K, Kikuchi K, Urano Y, Narazaki M, Yokawa T, Sakamoto S, Yamaguchi K, Nagano T. Chem Biol. 2002; 9:1027–1032. [PubMed: 12323377]
14. Zhang X, Lovejoy KS, Jasanoff A, Lippard SJ. Proc Natl Acad Sci USA. 2007; 104:10780–10785. [PubMed: 17578918]
15. Major JL, Parigi G, Luchinat C, Meade TJ. Proc Natl Acad Sci USA. 2007; 104:13881–13886. [PubMed: 17724345]
16. Bonnet CS, Caillé F, Pallier A, Morfin J-F, Petoud S, Suzenet F, Tóth É. Chem – Eur J. 2014; 20:10959–10969. [PubMed: 25116889]
17. Esqueda AC, López JA, Andreu-de-Riquer G, Alvarado-Monzón JC, Ratnakar J, Lubag AJM, Sherry AD, De León-´Rodríguez LM. J Am Chem Soc. 2009; 131:11387–11391. [PubMed: 19630391]
18. Lubag AJM, De Leon-Rodriguez LM, Burgess SC, Sherry AD. Proc Natl Acad Sci USA. 2011; 108:18400–18405. [PubMed: 22025712]
19. Sherry AD, Wu Y. Curr Opin Chem Biol. 2013; 17:167–174. [PubMed: 23333571]
20. Kotek J, Lebdušková P, Hermann P, Vander Elst L, Muller RN, Geraldes CFGC, Maschmeyer T, Lukes I, Peters JA. Chem – Eur J. 2003; 9:5899–5915. [PubMed: 14673862]
21. Zhang S, Kovacs Z, Burgess S, Aime S, Terreno E, Sherry AD. Chem – Eur J. 2001; 7:288–296. [PubMed: 11205022]
22. Siriwardena-Mahanama BN, Allen MJ. Molecules. 2013; 18:9352–9381. [PubMed: 23921796]
23. Jaszberenyi Z, Sour A, Toth E, Benmelouka M, Merbach AE. Dalton Trans. 2005:2713–2719. [PubMed: 16075110]
24. Congreve A, Parker D, Gianolio E, Botta M. Dalton Trans. 2004:1441–1445. [PubMed: 15252639]
25. Powell DH, Dhubhghaill OMN, Pubanz D, Helm L, Lebedev YS, Schlaepfer W, Merbach AE. J Am Chem Soc. 1996; 118:9333–9346.

26. Merbach, AE., Helm, L., Toth, E. The Chemistry of Contrast Agents in Medical Magnetic Resonance Imaging. 2nd. John Wiley & Sons, Ltd; West Sussex, U.K: 2013.
27. Champmartin D, Rubini P. Inorg Chem. 1996; 35:179–183. [PubMed: 11666182]
28. Martins AF, Morfin J-F, Geraldes CFGC, Tóth É. JBIC J Biol Inorg Chem. 2014; 19:281–295. [PubMed: 24297602]
29. Djanashvili K, Peters JA. Contrast Media Mol Imaging. 2007; 2:67–71. [PubMed: 17451189]
30. Botta M. Eur J Inorg Chem. 2000; 2000:399–407.
31. Caravan P, Cloutier NJ, Greenfield MT, McDermid SA, Dunham SU, Bulte JWM, Amedio JC Jr, Looby RJ, Supkowski RM, Horrocks WD Jr, McMurry TJ, Lauffer RB. J Am Chem Soc. 2002; 124:3152–3162. [PubMed: 11902904]
32. Tóth É, Connac F, Helm L, Adzamli K, Merbach AE. JBIC J Biol Inorg Chem. 1998; 3:606–613.
33. Adzamli K, Elst LV, Laurent S, Muller RN. MAGMA. 2001; 12:92–95. [PubMed: 11390262]
34. Henrotte V, Laurent S, Gabelica V, Elst LV, Depauw E, Muller RN. Rapid Commun Mass Spectrom. 2004; 18:1919–1924. [PubMed: 15329857]
35. Zech SG, Eldredge HB, Lowe MP, Caravan P. Inorg Chem. 2007; 46:3576–3584. [PubMed: 17425306]
36. Gale EM, Zhu J, Caravan P. J Am Chem Soc. 2013; 135:18600–18608. [PubMed: 24088013]
37. Montgomery CP, New EJ, Parker D, Peacock RD. Chem Commun. 2008:4261–4263.
38. Polasek M, Caravan P. Inorg Chem. 2013; 52:4084–4096. [PubMed: 23517079]
39. Brücher, E., Tircsó, G., Baranyai, Z., Kovács, Z., Sherry, AD. The Chemistry of Contrast Agents in Medical Magnetic Resonance Imaging. Merbach, A.Helm, L., Tóth, É., editors. John Wiley & Sons, Ltd; West Sussex, U.K.: 2013. p. 157-208.
40. Laurent S, Vander Elst L, Henoumont C, Muller RN. Contrast Media Mol Imaging. 2010; 5:305–308. [PubMed: 20803503]
41. Masuoka J, Hegenauer J, Dyke BRV, Saltman P. J Biol Chem. 1993; 268:21533–21537. [PubMed: 8408004]
42. Cousins RJ. Clin Physiol Biochem. 1986; 4:20–30. [PubMed: 2420502]

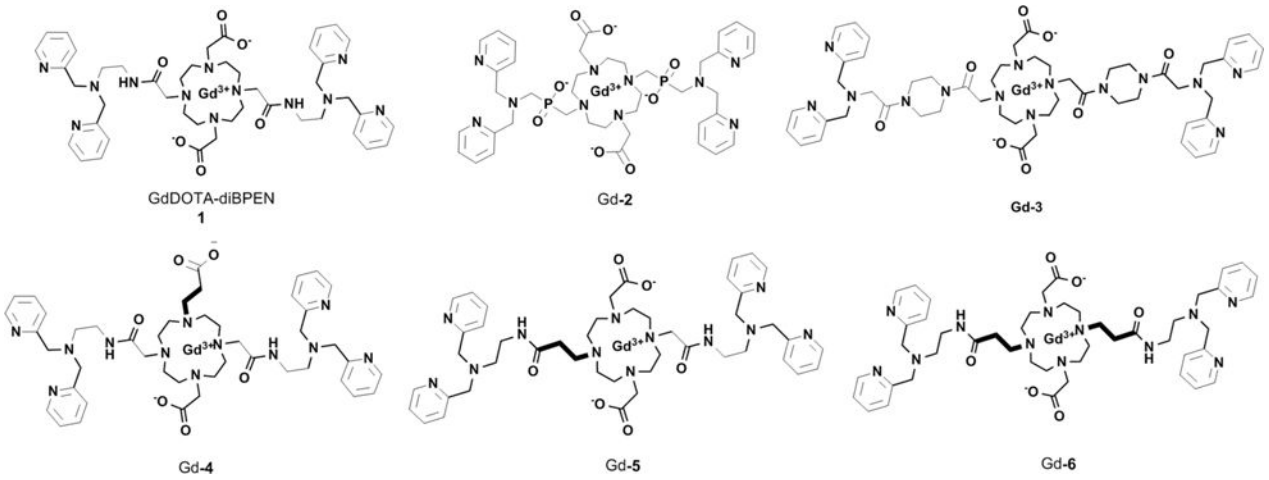

Figure 1.

Chemical structures of GdDOTA-diBPEN **1** and the modified Zn(II) sensors Gd-**2**-**6** reported in this work.

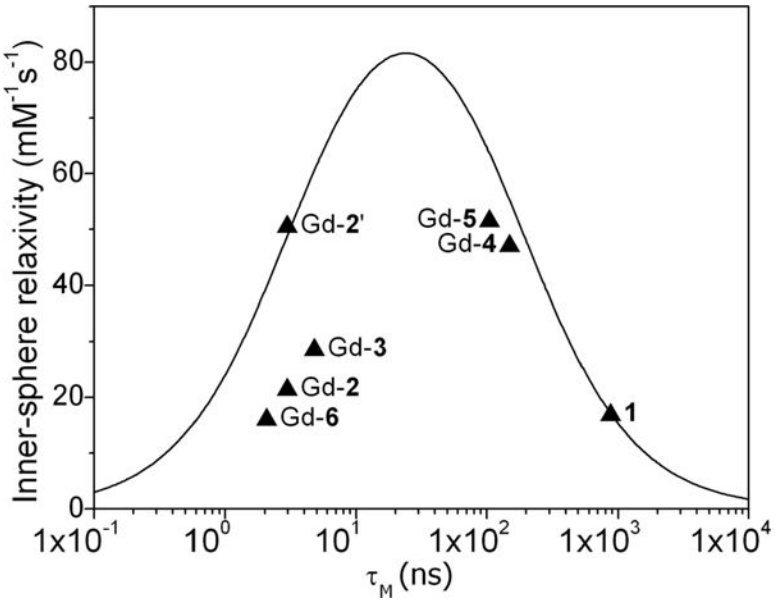

Figure 2.

Plot of r_1 for each Zn(II) sensor when bound to HSA versus τ_M measured for each unbound complexes in aqueous buffer at 310 K. The solid line shows the relationship predicted by paramagnetic relaxation theory at 0.47 T for a molecule with τ_R = 10 ns. The data point labeled Gd-**2**′ is the relaxivity value for Gd-**2** (q = 0.4) after normalization to q = 1. Other parameters used in calculating the theoretical curve include $r_{Gd–O}$ = 3.1 Å, q = 1 and T_{1e} = 5 ns.

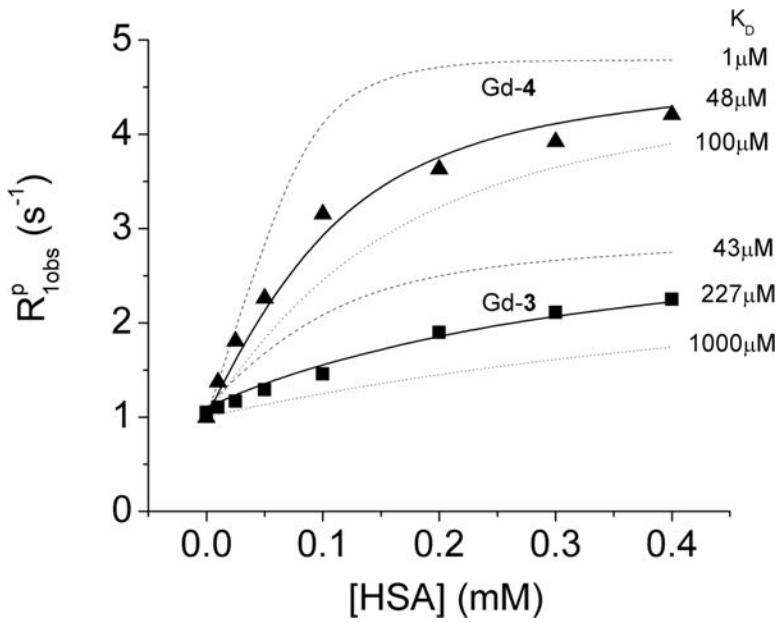

Figure 3.

Proton relaxation enhancement of Gd-**3**-$(Zn(II))_2$ and Gd-**4**-$(Zn(II))_2$ as a function of increasing concentration of HSA at 0.47 *T* and 310 K in 100 mM Tris buffer at pH 7.5. The solid line is the best fit of the data to eq 1, whereas the dashed and dotted lines are simulated curves for a fixed fully bound r_1 relaxivity (29.7 mM^{-1} s^{-1} for Gd-**3** and 48.4 mM^{-1} s^{-1} for Gd-**4**) with different dissociation constants (K_D). The simulated curves illustrate the sensitivity of the PRE method to variations in K_D.

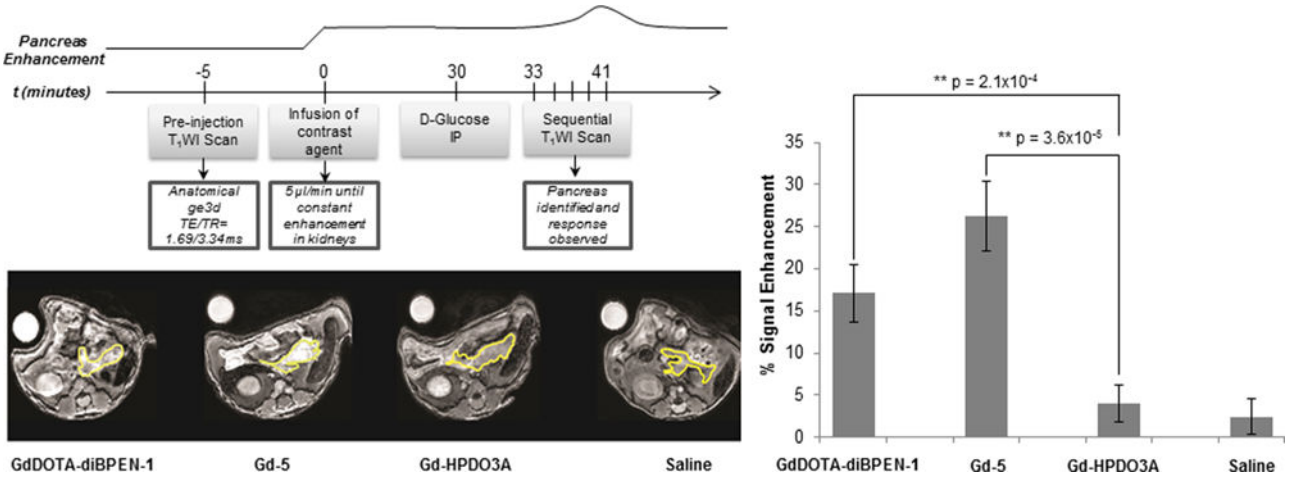

Figure 4.

Comparison of normalized signal enhancement in pancreatic tissues of mice after infusion of two different Zn(II) sensors followed by a bolus of glucose to stimulate insulin secretion. The images were collected at 11 min post glucose injection. The top panel shows the time-dependent infusion protocol. Gd-HPDO3A (ProHance) and saline were used as controls. The portion of the pancreas that could be identified in these slices is outlined in yellow. The bar graph shows the percent signal enhancement of normalized pancreatic tissue calculated from ROIs of images before and after glucose stimulation ($n = 5$).

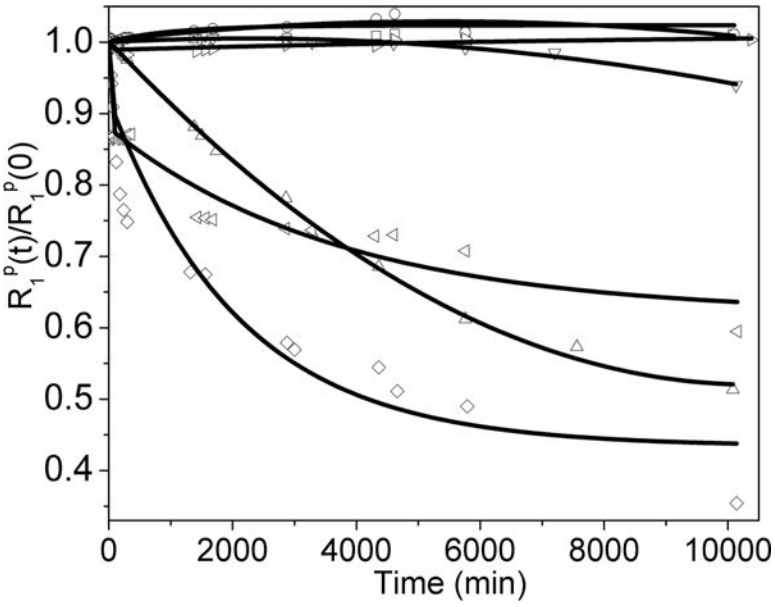

Figure 5.

Normalized T_1 relaxivity rates for GdDOTA-diBPEN **1**: 1 = ▷, Gd-**2** = □, Gd-**3** = ○, Gd-**4** = △, Gd-**5** = ▽, Gd-**6** = ◁, and GdDTPA = ◇ as a function of time. Each complex was initially 1.5 mM in 30 mM sodium phosphate buffer (pH = 7) in the presence of 6 mM of Zn(II). The samples were maintained at 310 K. The symbols correspond to experimental data points, whereas the solid lines represent a biexponential fit of the experimental data.

Table 1

Fitted Physical Parameters, HSA Binding Constants, and r_1 Relaxivities, in $mM^{-1}\ s^{-1}$, Measured at 0.47 *T* at 310 K

	GdDOTA-diBPEN 1	Gd-2	Gd-3	Gd-4	Gd-5	Gd-6
q	1.0 ± 0.2	0.4 ± 0.2	1.0 ± 0.2	1.0 ± 0.2	1.0 ± 0.2	0.9 ± 0.2
τ_{RO}^{298} (ns)	0.4 ± 0.1	0.3 ± 0.1	0.4 ± 0.1	0.3 ± 0.1	0.3 ± 0.1	0.3 ± 0.1
k_{ex}^{298} ($10^6\ s^{-1}$)/k_{ex}^{310} ($10^6\ s^{-1}$)	0.72 ± 0.1/1.1 ± 0.1	220 ± 2/350 ± 3	110 ± 2/250 ± 1	5.3 ± 0.2/6.3 ± 0.2	7.8 ± 0.1/9.2 ± 0.1	270 ± 3/490 ± 4
$^{298}\tau_M$ (ns)/$^{310}\tau_M$ (ns)	1400 ± 100/910 ± 60	4.5 ± 0.1/2.8 ± 0.1	8.7 ± 0.1/4.0 ± 0.1	190 ± 7/160 ± 5	130 ± 2/110 ± 1	3.7 ± 0.1/2.0 ± 0.1
r_1 ($mM^{-1}\ s^{-1}$)	5.0 ± 0.1	3.7 ± 0.1	7.6 ± 0.3	6.4 ± 0.2	6.2 ± 0.2	4.1 ± 0.1
$r_{1,sensor+2Zn(II)}$ ($mM^{-1}\ s^{-1}$)	6.6 ± 0.1	4.9 ± 0.2	6.5 ± 0.1	7.0 ± 0.2	7.0 ± 0.3	3.5 ± 0.1
$r_{1,sensor+2Zn(II)+albumin}$ ($mM^{-1}\ s^{-1}$	17.4 ± 0.5	20.8 ± 0.5	27.9 ± 0.8	47.6 ± 1.2	50.1 ± 1.2	15.6 ± 0.6
K_D with HSA (μM)[a]	42[b]	383 ± 60	227 ± 52	48 ± 15	42 ± 15	130 ± 25
r_1^c ($mM^{-1}\ s^{-1}$)[a]		23.8 ± 2	29.7 ± 1	48.4 ± 10	54.8 ± 7	14.2 ± 1

[a]Obtained by fitting proton relaxation enhancement data to **1**.

[b]From ref 17.